Oxidative-addition Reactions of $[W_2(\eta\text{-}C_5H_4R)_2X_4]$ (R = Pr^i or Me; X = Cl or Br): Reversible Addition of Dihydrogen to a Tungsten–Tungsten Triple Bond and X-Ray Crystal Structures of $[W_2(\eta\text{-}C_5H_4Pr^i)_2Cl_4(\mu\text{-}H)(\mu\text{-}PPh_2)]$ and $[W_2(\eta\text{-}C_5H_4Pr^i)_2Cl_3(\mu\text{-}Cl)(\mu\text{-}H)(\mu\text{-}PPh_2)(PMe_3)]$ *

Qian Feng,[a] Montserrat Ferrer,[a] Malcolm L. H. Green,[a] Philip Mountford,[a] Victor S. B. Mtetwa[b] and Keith Prout[c]

[a] *Inorganic Chemistry Laboratory, South Parks Road, Oxford OX1 3QR, UK*

[b] *University of Swaziland, P/B 4, Kwaluseni, Manzini, Swaziland*

[c] *Chemical Crystallography Laboratory, 9 Parks Road, Oxford OX1 3PD, UK*

The unsupported W≡W bond of $[W_2(\eta\text{-}C_5H_4R)_2X_4]$ (X = Cl, R = Pr^i **1a** or Me **1b**; X = Br, R = Pr^i **2**) readily undergoes oxidative-addition reactions with HY [Y = H, Cl, SR′ (R′ = Me, Et, Pr^i, Ph or Bu^t), or PPhR′ (R′ = H or Ph)] to afford the corresponding derivatives $[W_2(\eta\text{-}C_5H_4R)_2X_4(\mu\text{-}H)(\mu\text{-}Y)]$ in good yields. For **1a** the addition of H_2 is reversible with reductive elimination occurring readily at *ca.* 50 °C under reduced pressure. The μ-phosphido complex $[W_2(\eta\text{-}C_5H_4Pr^i)_2Cl_4(\mu\text{-}H)(\mu\text{-}PPh_2)]$ has been crystallographically characterised and possesses a W=W double bond [2.6558(3) Å]. The μ-thiolato complexes $[W_2(\eta\text{-}C_5H_4R)_2Cl_4(\mu\text{-}H)(\mu\text{-}SR')]$ are fluxional and undergo inversion at the μ-S atom; $\Delta G^{\ddagger}$ values for this process have been determined and increase in the order R′ = Bu^t < Pr^i < Ph < Et < Me. The μ-chloro complexes $[W_2(\eta\text{-}C_5H_4R)_2Cl_4(\mu\text{-}Cl)(\mu\text{-}H)]$ undergo a different fluxional process which effectively involves rotation of the (μ-Cl)(μ-H) fragment about the W–W vector. The complexes $[W_2(\eta\text{-}C_5H_4Pr^i)_2Cl_4(\mu\text{-}H)(\mu\text{-}Y)]$ (Y = H or PPh_2) react with PMe_3 to give the corresponding adducts $[W_2(\eta\text{-}C_5H_4Pr^i)_2Cl_3(\mu\text{-}Cl)(\mu\text{-}H)(\mu\text{-}Y)(PMe_3)]$, the X-ray crystal structure of the μ-phosphido complex (Y = PPh_2) having been determined. In contrast, treatment of $[W_2(\eta\text{-}C_5H_4Pr^i)_2Cl_4(\mu\text{-}H)(\mu\text{-}Y)]$ (Y = Cl or SR′) with an excess of PMe_3 affords the mononuclear complex $[W(\eta\text{-}C_5H_4Pr^i)Cl(PMe_3)_3]$.

We recently reported the synthesis of the W≡W triply bonded dimers $[W_2(\eta\text{-}C_5H_4R)_2X_4]$ (X = Cl, R = Pr^i **1a** or Me **1b**; X = Br, R = Pr^i **2**)[1] and the reactions of **1** with alkynes.[2] A molecular orbital and photoelectron spectroscopic study of **1a** found a valence electronic description of $(\sigma^2)(\pi^4)$ for the W≡W triple bond and a first ionisation energy[3] of 6.48 eV (*ca.* 10.4×10^{-19} J) suggesting that the complexes **1** and **2** might undergo oxidative-addition reactions in a manner comparable to that of other metal–metal multiply bonded complexes.[4] Here we report the oxidative-addition reactions of $[W_2(\eta\text{-}C_5H_4R)_2X_4]$ with HY [Y = H, Cl, PHR′ (R′ = H or Ph) or SR′ (R′ = Me, Et, Pr^i, Ph or Bu^t)]. Part of this work has been communicated.[5]

Results and Discussion

Reaction with H_2.—When toluene solutions of complex **1a** or **2** were treated with H_2 (2–3 atm) at room temperature for several hours a colour change from emerald green to turquoise was observed. Reduction in volume and addition of light petroleum afforded microcrystals of the μ-hydrido derivative $[W_2(\eta\text{-}C_5H_4Pr^i)_2X_4(\mu\text{-}H)_2]$ (X = Cl, **3**; or Br, **4**). The new compounds **3** and **4** were characterised by elemental analysis and by NMR spectroscopy. Characterising data for **3** and **4** and all the other new compounds described herein are given in Table 1, and the proposed structures are shown in Scheme 1. The NMR spectra show resonances assignable to an $\eta\text{-}C_5H_4Pr^i$ moiety, and a single sharp resonance at δ *ca.* 1.2 integrating as one H atom per $\eta\text{-}C_5H_4Pr^i$ ligand and which shows a large coupling to ^{183}W (^{183}W, $I = \frac{1}{2}$, natural abundance = 14.5%) with the proper satellite intensity for a hydride ligand bridging two W atoms. Furthermore, the latter resonance is absent for the otherwise identical isotopomer $[^2H_2]$ **3** prepared from **1a** and D_2. The magnitude of $^1J(^1H\text{–}^{183}W)$ (112–116 Hz) and the low-temperature T_1 value for **3** (*ca.* 1.2 s at −90 °C) militate in favour of a $W(\mu\text{-}H)_2W$ unit rather than the alternative molecular dihydrogen formulation $W(\mu\text{-}H_2)W$.[6] There is no evidence for a terminal hydride ligand in the IR spectra of either **3** or **4**. From these data we propose that complexes **3** and **4** possess the binuclear, hydride-bridged structures shown in Scheme 1. Although the spectroscopic data do not rule out an alternative *cis* disposition of the $\eta\text{-}C_5H_4Pr^i$ rings, the solid-state structures of $[Re_2(\eta\text{-}C_5Me_4Et)_2H_4(\mu\text{-}H_2)]$[7] and $[W_2(\eta\text{-}C_5H_4Pr^i)_2Cl_4(\mu\text{-}H)(\mu\text{-}PPh_2)]$ (see below) strongly suggest the *trans* relationship illustrated in Scheme 1.

Heating a $[^2H_8]$toluene solution of complex **3** at 50 °C under reduced pressure for *ca.* 30 min gave quantitative recovery of **1a** and a sharp resonance at δ 4.45 (assignable to free H_2) as monitored by ^1H NMR spectroscopy. To our knowledge this is the first example of the reversible addition of dihydrogen to a metal–metal multiple bond. In contrast, the bromide-supported complex **4** does not undergo reductive elimination under these conditions. We note that the photo-

* μ-Diphenylphosphido-μ-hydrido-bis[dichloro(η-isopropylcyclopentadienyl)tungsten](2*W–W*) and μ-chloro-trichloro-1κ^2*Cl*,2κ*Cl*-μ-diphenylphosphido-μ-hydrido-bis[1,2(η)-isopropylcyclopentadienyl](trimethylphosphine-2κ*P*)ditungsten–dichloromethane (1/1).

Supplementary data available: see Instructions for Authors, *J. Chem. Soc., Dalton Trans.*, 1991, Issue 1, pp. xviii–xxii.

Non-SI units employed: atm = 101 325 Pa, cal = 4.184 J.

Table 1 Analytical and spectroscopic data

Compound	Colour	Analysis (%)[a] C	H	Halide	NMR data[b]
3	Turquoise	26.2 (26.5)	3.2 (3.3)	19.3 (19.5)	^{1}H: 7.01, 5.15 (2 × virtual t, 2 × 4 H, *J* 2.4, η-C$_5$*H*$_4$Pr^i), 2.44 (spt, 2 H, *J* 6.9, C*H*Me$_2$), 1.24 [s, 2 H, ^1J(^{1}H–^{183}W) 113 (*ca.* 25% by area), W(μ-H)$_2$W], 0.75 (d, 12 H, *J* 6.9, CH*Me*$_2$) ^{13}C: 138.0 (s, *C*Pr^i), 106.3 (d, *J* 179, *C*H of η-*C*$_5$H$_4$Pr^i), 101.2 (d, *J* 185, *C*H of η-*C*$_5$H$_4$Pr^i), 28.2 (d, *J* 132, *C*HMe$_2$), 21.9 (q, *J* 126, CH*Me*$_2$)
4	Green	21.2 (21.5)	2.6 (2.5)	35.8 (35.5)	^{1}H: 6.99, 5.19 (2 × virtual t, 2 × 4 H, *J* 2.4, η-C$_4$*H*$_4$Pr^i), 2.57 (spt, 2 H, *J* 6.9, C*H*Me$_2$), 1.16 [s, 2 H, ^1J(^{1}H–^{183}W) 116.4 (*ca.* 26% by area), W(μ-H)$_2$W], 0.77 (d, 12 H, *J* 6.9, CH*Me*$_2$)
5a	Red-brown	25.4 (25.3)	3.05 (3.05)	23.1 (23.3)	^{1}H:[c,d] 6.90, 6.54, 5.67, 5.30 (4 × br m, 4 × 2 H, η-C$_5$*H*$_4$Pr^i), 2.55 (spt, 2 H, *J* 6.9, C*H*Me$_2$), 1.13 (d, 12 H, *J* 6.9, CH*Me*$_2$), −1.89 [s, 1 H, ^1J(^{1}H–^{183}W) 92 (24% by area), W(μ-H)W] ^{13}C-{^{1}H}:[c,e] 138.6 (*C*Pr^i), 106.6, 105.2, 96.6 (4 × CH of η-*C*$_5$H$_4$Pr^i, two signals overlapping), 28.3 (*C*HMe$_2$), 22.1, 21.7 (2 × CH*Me*$_2$)
5b	Red-brown	20.8 (20.5)	2.2 (2.15)	24.2 (25.2)	^{1}H:[c,d] 7.07, 6.33, 5.56, 5.53 (4 × br m, 4 × 2 H, η-C$_5$*H*$_4$Me), 2.06 (6 H, Me), −1.84 [s, 1 H, ^1J(^{1}H–^{183}W) 93 (*ca.* 25% by area), W(μ-H)W]
6a	Red	37.1 (36.9)	3.6 (3.65)	15.6 (15.6)	^{1}H:[c] 8.03, 7.51 (2 × m, 2 × 4 H, *o*- and *m*-H of C$_6$H$_5$), 7.40 (m, 2 H, *p*-H of C$_6$H$_5$), 6.46 (virtual q, 2 H, *J* 2.4, η-C$_5$*H*$_4$Pr^i), 5.27 (overlapping 2 × virtual q, 4 H, η-C$_5$H$_4$Pr^i), 4.44 (virtual q, 2 H, *J* 2.4, η-C$_5$*H*$_4$Pr^i), 2.49 (spt, 2 H, *J* 6.9, C*H*Me$_2$), 1.13, 0.95 (2 × d, 2 × 6 H, *J* 6.9, CH*Me*$_2$), −1.86 [d, 1 H, ^2J(^{1}H–^{31}P) 6.1, ^1J(^{1}H–^{183}W) 89 (*ca.* 24% by area), W(μ-H)W] ^{13}C-{^{1}H}:[c] 144.8 [d, ^1J(^{13}C–^{31}P) 52, *ipso*-C of C$_6$H$_5$], 138.2 (*C*Pr^i), 134.2, 130.5, 128.2 (*o*-, *m*- and *p*-C of C$_6$H$_5$), 113.3, 101.5, 98.0, 97.0 (4 × CH of η-C$_5$H$_4$Pr^i), 28.0 (*C*HMe$_2$), 22.3, 20.8 (2 × CH*Me*$_2$) ^{31}P-{^{1}H}:[c] 263 [^1J(^{31}P–^{183}W) 248 (*ca.* 28% by area), μ-PPh$_2$]
6b[f]	Red-brown	32.5 (32.8)	2.9 (2.9)	20.1 (19.8)	^{1}H:[c] 7.98, 7.50 (2 × m, 2 × 4 H, *o*- and *m*-H of C$_6$H$_5$), 7.38 (m, 2 H, *p*-H of C$_6$H$_5$), 6.26, 5.54, 5.28, 4.26 (4 × virtual q, 4 × 2 H, *J* 2.4, η-C$_5$*H*$_4$Me), 1.69 (overlapping 2 × s, 6 H, Me), −1.77 [d, 1 H, ^2J(^{1}H–^{31}P) 6, ^1J(^{1}H–^{183}W) 89.7 (*ca.* 25% by area), W(μ-H)W] ^{31}P-{^{1}H}:[c] 264.0 [^1J(^{31}P–^{183}W) 255.1 (*ca.* 25% by area), μ-PPh$_2$]
7	Red-brown	31.7 (31.8)	3.2 (3.15)	29.6 (30.2)	^{1}H:[c] 8.07, 7.50 (2 × m, 2 × 4 H, *o*- and *m*-H of C$_6$H$_5$), 7.40 (m, 2 H, *p*-H of C$_6$H$_5$), 6.69, 5.24, 4.79, 4.57 (4 × virtual q, 4 × 2 H, *J* 2.4, η-C$_5$*H*$_4$Pr^i), 2.74 (spt, 2 H, *J* 6.9, C*H*Me$_2$), 1.15, 1.02 (2 × d, 2 × 6 H, *J* 6.9, CH*Me*$_2$), −2.58 [d, 1 H, ^2J(^{1}H–^{31}P) 6.5, ^1J(^{1}H–^{183}W) 92 (*ca.* 26% by area), W(μ-H)W] ^{31}P-{^{1}H}:[c] 271.6 [^1J(^{31}P-^{183}W) 248 (*ca.* 24% by area), η-PPh$_2$]
8a	Red-brown	31.6 (31.7)	3.5 (3.5)	17.2 (17.0)	^{1}H: 10.45 [d, 1 H, ^1J(^{1}H–^{31}P) 428, μ-P*H*Ph], 7.88, 7.05 (2 × m, 2 H + 3 H, C$_6$H$_5$), 6.43, 6.38, 5.88, 5.67, 5.17, 5.12, 4.82, 4.44 (8 × m, 8 × 1 H, η-C$_5$*H*$_4$Pr^i), 2.47 (overlapping 2 × spt, 2 H, C*H*Me$_2$), 0.85–0.75 (overlapping 3 × d, 9 H, CH*Me*$_2$), 0.72 (d, 3 H, *J* 6.9, CH*Me*$_2$), −1.32 [d, 1 H, ^2J(^{1}H–^{31}P) 5.4, ^1J(^{1}H–^{183}W) 99.1 and 95.3 (*ca.* 26% by combined area), W(μ-H)W] ^{13}C-{^{1}H}:[c] 137.5 [d, ^1J(^{13}C–^{31}P) 57, *ipso*-C of C$_6$H$_5$], 137.2, 136.4 (2 × *C*Pr^i), 134.8, 132.2, 128.9 (*o*-, *m*- and *p*-C of C$_6$H$_5$), 106.0, 105.9, 102.1, 101.4, 96.9, 94.4, 92.9 (8 × CH of η-*C*$_5$H$_4$Pr^i; two signals overlapping), 28.0 (2 × *C*HMe$_2$, 2 signals overlapping), 22.5, 22.1, 21.4, 20.9 (4 × CH*Me*$_2$) ^{31}P-{^{1}H}:[c] 263.5 [^1J(^{31}P–^{183}W) 234.8 and 218.3 (*ca.* 26% by combined area), μ-PHPh]
8b	Red-brown	28.1 (27.8)	2.6 (2.7)	18.4 (18.2)	^{1}H:[c] 10.58 [d, 1 H, ^1J(^{1}H–^{31}P) 431.4, μ-P*H*Ph], 7.88, 7.57 (2 × m, 2 H + 3 H, C$_6$H$_5$), 6.55, 6.27, 6.18, 6.08, 5.41, 5.34, 4.78 (7 × br m, 8 × 1 H, η-C$_5$*H*$_4$Me, two signals overlapping), 1.96, 1.91 (2 × s, 2 × 3 H, Me), −1.73 [d, 1 H, ^2J(^{1}H–^{31}P) 5.4, ^1J(^{1}H–^{183}W) 100.4 and 86.3 (*ca.* 27% by combined area), W(μ-H)W] ^{31}P-{^{1}H}:[c] 253.8 [^1J(^{31}P-^{183}W) 238.1 and 220.4 (*ca.* 26% by combined area), μ-PHPh]
9a	Brown	27.0 (26.7)	3.4 (3.4)	18.1 (18.3)	^{1}H: 6.34, 6.26, 6.18, 6.00, 5.04 (5 × virtual q, 5 × 1 H, *J* 2.4, η-C$_5$*H*$_4$Pr^i), 4.95 (overlapping 2 × virtual q, 2 H, η-C$_5$*H*$_4$Pr^i), 4.62 (virtual q, 1 H, *J* 2.4, η-C$_5$*H*$_4$Pr^i), 2.87 (s, 3 H, SMe), 2.47 (overlapping 2 × spt, 2 H, C*H*Me$_2$), 0.88, 0.86, 0.81, 0.79 (4 × d, 4 × 3 H, *J* 6.9, CH*Me*$_2$), −1.87 [s, 1 H, ^1J(^{1}H–^{183}W) 96 (*ca.* 24% by area), W(μ-H)W] ^{13}C-{^{1}H}: 138.8, 137.9 (2 × *C*Pr^i), 106.5, 105.4, 104.1, 103.7, 97.5, 95.9, 95.7, 94.8 (8 × CH of η-*C*$_5$H$_4$Pr^i), 28.1 (2 × *C*HMe$_2$, 2 signals overlapping), 24.5 (SMe), 22.0, 21.9, 21.2 (4 × CH*Me*$_2$, 2 signals overlapping)
9b	Red-brown	21.65 (21.8)	2.45 (2.5)	20.1 (19.8)	^{1}H:[c] 6.71, 6.63, 6.43, 6.17, 5.53, 5.31, 5.25, 5.10 (8 × virtual q, 8 × 1 H, *J* 2.4, η-C$_5$*H*$_4$Pr^i), 3.34 (s, 3 H, SMe), 2.04, 1.98 (2 × s, 2 × 3 H, η-C$_5$H$_4$*Me*), −2.22 [s, 1 H, ^1J(^{1}H–^{183}W) 95.4 (*ca.* 25% by area), W(μ-H)W]
10a	Red-brown	27.9 (27.6)	3.6 (3.6)	18.5 (18.1)	^{1}H: 6.66, 6.61, 6.59, 6.20, 5.60, 5.27 (6 × virtual q, 6 × 1 H, *J* 2.4, η-C$_5$*H*$_4$Pr^i), 5.20 (overlapping 2 × virtual q, 2 H, η-C$_5$*H*$_4$Pr^i), 4.32, 3.04 (2 × d of q, 2 × 1 H, ^2J 12.7, ^3J 7.3, SC*H*$_2$Me), 2.50 (overlapping 2 × spt, 2 H, C*H*Me$_2$), 1.59 (t, 3 H, *J* 7.3, SCH$_2$*Me*), 1.15–1.05 (overlapping 4 × d, 12 H, CH*Me*$_2$), −2.36 [s, 1 H, ^1J(^{1}H–^{183}W) 96 (*ca.* 24% by area), W(μ-H)W] ^{13}C-{^{1}H}: 137.8, 137.1 (2 × *C*Pr^i), 106.4, 105.6, 103.4, 103.1, 96.6, 95.9, 95.3, 94.3 (8 × CH of η-*C*$_5$H$_4$Pr^i), 35.1 (SCH$_2$Me), 28.1, 27.8 (2 × *C*HMe$_2$), 22.1, 21.8, 21.4, 21.1 (4 × CH*Me*$_2$), 17.3 (SCH$_2$*Me*)

Table 1 (*continued*)

Compound	Colour	Analysis (%)[a] C	H	Halide	NMR data[b]
10b[b]	Red-brown	22.5 (22.8)	2.6 (2.75)	22.0 (21.2)	^{1}H:[c] 6.44, 6.08, 5.54, 5.29, 5.22, 5.12 (6 × virtual q, 6 × 1 H, *J* 2.4, η-C$_5$*H*$_4$Me),[h] 4.31, 3.03 (2 × d of q, 2 × 1 H, ^{2}*J* 14.3, ^{3}*J* 7.4, SC*H*$_2$Me), 2.01, 1.97 (2 × s, 2 × 3 H, η-C$_5$H$_4$*Me*), 1.57 (t, 3 H, *J* 7.4, SCH$_2$*Me*), −2.26 [s, 1 H, ^{1}*J*(^{1}H–^{183}W) 95.5 (*ca.* 26% by area), W(μ-H)W]
11a	Red-brown	31.6 (31.7)	3.35 (3.4)	16.0 (17.0)	^{1}H:[d,i] 7.96 (d, 2 H, *J* 7.5 *o*-H of C$_6$H$_5$),[j] 6.43, 6.33, 6.17, 5.89, 5.19, 5.07, 4.89, 4.20 (8 × virtual q, 8 × 1 H, *J* 2.4, η-C$_5$*H*$_4$Pr^i), 2.44 (overlapping 2 × spt, 2 H, C*H*Me$_2$), 1.0–0.75 (overlapping 4 × d, 12 H, CH*Me*$_2$), −1.77 [s, 1 H, ^{1}*J*(^{1}H–^{183}W) 95.1 and 90.7 (*ca.* 26% by combined area), W(μ-H)W] ^{13}C-{^{1}H}:[c] 139.1, 138.1 (2 × *C*Pr^i), 136.4 (*ipso*-C of C$_6$H$_5$), 135.2, 130.7, 128.9 (*o*-, *m*- and *p*-C of C$_6$H$_5$), 110.1, 108.2, 104.7, 103.2, 98.5, 97.0, 96.7, 95.4 (8 × CH of η-C$_5$H$_4$Pr^i), 28.2 (2 × *C*HMe$_2$; 2 signals overlapping), 22.3, 21.9, 21.7, 20.6 (4 × CH*Me*$_2$)
11b	Red-brown	27.5 (27.8)	2.5 (2.6)	18.9 (18.2)	^{1}H:[c] 7.79 (d, 2 H, *J* 7.8, *o*-H of C$_6$H$_5$), 7.51 (overlapping d and t, 3 H, *m*- and *p*-H of C$_6$H$_5$), 6.75, 6.42, 6.34, 6.25, 5.60 (5 × br signals, 5 × 1 H, η-C$_5$H$_4$Me), 5.40 (overlapping 2 × br signals, 2 H, η-C$_5$*H*$_4$Me), 4.58 (br signal, 1 H, η-C$_5$*H*$_4$Me), 2.06, 1.91 (2 × s, 2 × 3 H, η-C$_5$H$_4$*Me*), −2.01 [s, 1 H, ^{1}*J*(^{1}H–^{183}W) 87.1 (*ca.* 26% by area), W(μ-H)W]
12a	Red-brown	28.4 (28.6)	3.9 (3.8)	18.0 (17.7)	^{1}H:[c,d] 7.01, 6.87, 6.49, 5.90, 5.54, 5.38, 5.29, 5.08 (8 × br m, 8 × 1 H, η-C$_5$*H*$_4$Pr^i), 4.09 (spt, 1 H, *J* 6.3, SC*H*Me$_2$), 2.47, 2.32 (2 × spt, 2 × 1 H, *J* 6.9, C*H*Me$_2$ of η-C$_5$H$_4$Pr^i), 1.67, 1.51 (2 × d, 2 × 3 H, *J* 6.3, SCH*Me*$_2$), 1.15–0.95 (4 × overlapping d, 12 H, CH*Me*$_2$ of η-C$_5$H$_4$Pr^i), −2.51 [s, 1 H, ^{1}*J*(^{1}H–^{183}W) 96 (*ca.* 24% by area), W(μ-H)W] ^{13}C-{^{1}H}:[c,d] 139.0, 136.8 (*C*Pr^i), 110.4, 105.2, 103.2, 101.8, 96.9, 95.9, 95.4, 93.4 (8 × CH of η-*C*$_5$H$_4$Pr^i), 44.9 (S*C*HMe$_2$), 28.3, 27.9 (2 × *C*HMe$_2$ of η-*C*$_5$H$_4$Pr^i), 25.9, 24.8 (2 × SCH*Me*$_2$), 22.7, 21.8, 21.5, 20.9 (4 × CH*Me*$_2$ of η-C$_5$H$_4$Pr^i)
12b	Dark red	24.4 (24.2)	2.9 (3.0)	19.8 (19.1)	^{1}H:[c,e] 7.26, 6.80, 6.18, 5.82, 5.58, 5.34, 5.21, 5.15 (8 × br m, 8 × 1 H, η-C$_5$*H*$_4$Me), 4.05 (spt, 1 H, *J* 6.3, SC*H*Me$_2$, 1.91, 1.90 (2 × s, 2 × 3 H, η-C$_5$H$_4$*Me*), 1.64, 1.47 (2 × d, 2 × 3 H, *J* 6.3, SCH*Me*$_2$), −2.38 [s, 1 H, ^{1}*J*(^{1}H–^{183}W) 95.3 (*ca.* 25% by area), W(μ-H)W]
13a	Red-brown	29.5 (29.5)	3.9 (3.95)	17.7 (17.4)	^{1}H: 6.98 (overlapping 2 × virtual q, 4 H, η-C$_5$*H*$_4$Pr^i), 5.68, 5.61 (2 × virtual q, 2 × 2 H, *J* 2.4, η-C$_5$*H*$_4$Pr^i), 3.12 (spt, 2 H, *J* 6.9, C*H*Me$_2$), 2.36 (s, 9 H, SBu^t), 1.51, 1.48 (2 × d, 2 × 6 H, *J* 6.9, CH*Me*$_2$), −1.49 [s, 1 H, ^{1}*J*(^{1}H–^{183}W) 94 (*ca.* 26% by area), W(μ-H)W] ^{13}C-{^{1}H}:[c,k] 139.7 (*C*Pr^i), 106.4, 102.6, 95.4, 93.0 (4 × CH of η-*C*$_5$H$_4$Pr^i), 65.1 (S*C*Me$_3$), 33.2 (SC*Me*$_3$), 28.4 (*C*HMe$_2$), 22.3, 21.7 (2 × CH*Me*$_2$)
13b	Cherry-red	25.9 (25.4)	3.2 (3.2)	18.8 (18.7)	^{1}H:[c] 6.74, 6.27, 5.50, 5.25 (4 × virtual q, 4 × 2 H, *J* 2.4, η-C$_5$*H*$_4$Me), 2.01 (overlapping 2 × s, 6 H, η-C$_5$H$_4$*Me*), 1.82 (s, 9 H, SBu^t), −2.49 [s, 1 H, ^{1}*J*(H^1–^{183}W) 90.4 (*ca.* 25% by area), W(μ-H)W]
14	Red-brown	37.0 (37.1)	4.4 (4.4)	14.1 (14.4)	^{1}H:[c] 7.40–7.30, 7.25–7.15 (overlapping 2 × m, 2 × 5 H, C$_6$H$_5$), 5.03 (br virtual q, 1 H, η-C$_5$*H*$_4$Pr^i), 4.87 [d of virtual q, 1 H, ^{3}*J*(^{1}H–^{31}P) 11.9 (η-C$_5$*H*$_4$Pr^i)WCl$_2$(PMe$_3$)], 4.87 (overlapping 2 × br virtual q, 2 H, η-C$_5$*H*$_4$Pr^i), 4.50, 4.41, 4.05, 3.70 (4 × br virtual q, 4 × 1 H, η-C$_5$*H*$_4$Pr^i), 2.81, 2.68 (2 × spt, 2 × 1 H, *J* 6.9, C*H*Me$_2$), 2.34 [d of d, 1 H, ^{2}*J*(^{1}H–^{31}P) 16.8 (PMe$_3$) and 9.5 (PPh$_2$), W(μ-H)W], 1.71 [d, 9 H, ^{2}*J*(^{1}H–^{31}P) 9.8, PMe$_3$], 1.34 (d, 3 H, *J* 6.9, CH*Me*$_2$), 1.28 (d, 3 H, *J* 6.9, CH*Me*$_2$), 1.18 (overlapping 2 × d, 6 H, CH*Me*$_2$) ^{13}C-{^{1}H}:[c] 145.9, 142.5 [d, ^{1}*J*(^{13}C–^{31}P) 30.0, 2 × *ipso*-C of C$_6$H$_5$], 136.3, 135.9 (2 × *o*-, *m*- or *p*-C of C$_6$H$_5$), 134.3, 132.6 (2 × *C*Pr^i), 129.2, 128.7, 128.0, 127.3 (4 × *o*-, *m*- or *p*-C of C$_6$H$_5$), 97.9, 93.6, 93.2, 89.1, 87.1, 84.9, 80.3, 74.6 (8 × CH of η-*C*$_5$H$_4$Pr^i), 28.7, 28.5 (2 × *C*HMe$_2$), 24.2, 22.9, 22.3, 22.1 (4 × CH*Me*$_2$), 17.1 [d, ^{1}*J*(^{13}C–^{31}P) 31.3, PMe$_3$] ^{31}P-{^{1}H}:[c] 57 [d, *J* 83, ^{1}*J*(^{31}P–^{183}W) 254 (*ca.* 28% by area), W(μ-PPh$_2$)W], −27 ([d, *J* 83, ^{1}*J*(^{31}P–^{183}W) 259 (*ca.* 14% by area), PMe$_3$]
15	Purple	28.5 (28.45)	3.9 (4.1)	17.4 (17.7)	^{1}H: 5.63, 4.88 [2 × virtual q, 2 × 1 H, *J* 2.4, (η-C$_5$*H*$_4$Pr^i)WCl$_2$], 4.83 [br virtual q, 1 H, *J* 2.4, (η-C$_5$*H*$_4$Pr^i)WCl(PMe$_3$)], 4.80 [virtual q, 1 H, *J* 2.4, (η-C$_5$*H*$_4$Pr^i)WCl$_2$], 4.46, 4.38 [2 × br m, 2 × 1 H, (η-C$_5$*H*$_4$Pr^i)WCl(PMe$_3$)], 4.18 [virtual q, 1 H, *J* 2.4, (η-C$_5$*H*$_4$Pr^i)WCl$_2$], 3.71 [d of virtual q, 1 H, *J* 2.4, ^{3}*J*(^{1}H–^{31}P) 10.7, (η-C$_5$*H*$_4$Pr^i)WCl(PMe$_3$)], 2.70 (spt, 1 H, *J* 6.9, C*H*Me$_2$), 2.59 [d of d, 1 H, *J* 10.8, ^{2}*J*(^{1}H–^{31}P) 20.0, ^{1}*J*(^{1}H–^{183}W) 42.6 (*ca.* 23% by area), W(μ-H)W], 2.38 (spt, 1 H, *J* 6.9, C*H*Me$_2$), 1.28 [d, 9 H, ^{2}*J*(^{1}H–^{183}W) 8.5, PMe$_3$], 1.15, 1.06, 0.98, 0.94 (4 × d, 4 × 3 H, *J* 6.9, CH*Me*$_2$), −4.59 [d of d, 1 H, *J* 10.8, ^{2}*J*(^{1}H–^{31}P) 31.0, ^{1}*J*(^{1}H–^{183}W) 56 and 80 (*ca.* 26% by area), W(μ-H)W] ^{13}C-{^{1}H}: 135.9, 131.2 (2 × *C*Pr^i), 104.6, 98.2, 94.6, 90.0, 89.9, 89.5, 84.7, 82.0 (8 × CH of η-*C*$_5$H$_4$Pr^i), 28.9, 28.1 (2 × *C*HMe$_2$), 22.7, 22.2, 21.9, 21.3 (4 × CH*Me*$_2$), 19.2 [d, ^{1}*J*(^{13}C–^{31}P) 33, PMe$_3$] ^{31}P-{^{1}H}: −22.7 [^{1}*J*(^{31}P–^{183}W) 250.7 (*ca.* 15% by area), PMe$_3$]

Table 1 (*continued*)

Compound	Colour	Analysis (%)[a] C	H	Halide	NMR data[b]
16	Pale yellow	33.5 (33.8)	6.5 (6.6)	16.1 (16.6)	^{1}H:[c] 5.36, 4.98 (2 × m, 2 × 2 H, η-$C_5H_4Pr^i$), 2.64 (spt, 1 H, *J* 6.9, C*H*Me$_2$), 1.81 [d, 9 H, $^2J(^1H-^{31}P)$ 9.4, ClW(PMe$_3$)], 1.62 [virtual t, 18 H, $^2J(^1H-^{31}P)$ 9.6, (Me$_3$P)W(PMe$_3$)], 0.82 (d, 6 H, *J* 6.9, CH*Me*$_2$) ^{31}P-{^{1}H}:[c] −35.2 [t, 1 P, *J* 13.4, ClW(PMe$_3$)], −36.4 [d, 2 P, *J* 13.4 (Me$_3$P)W(PMe$_3$)]

[a] Calculated values given in parentheses; halide = Cl or Br as appropriate. [b] At 25 °C in [$^2H_6$]benzene unless stated otherwise. Data given as: chemical shift (δ), multiplicity (s = singlet, d = doublet, t = triplet, q = quartet, spt = septet, m = multiplet, br = broad), relative intensity, coupling constant (in Hz), and assignment; for virtual multiplets *J* is the *apparent* coupling constant; for ^{1}H, ^{13}C or ^{31}P NMR spectra *J* refers to the ^{1}H–^{1}H, ^{13}C–^{1}H or ^{31}P–^{31}P coupling constant respectively unless stated otherwise. [c] In [$^2H_2$]dichloromethane. [d] At −30 °C. [e] At −70 °C. [f] Analysis for **6b**·0.5CH_2Cl_2. [g] Analysis for **10b**·0.25CH_2Cl_2. [h] Two further η-C_5H_4Me resonances obscured by residual protio-solvent resonance. [i] In [$^2H_8$]toluene. [j] The *m*- and *p*-H resonances of C_6H_5 obscured by residual protio-solvent resonances. [k] At −15 °C.

Table 2 Selected bond lengths (Å) and angles (°) for [W_2(η-$C_5H_4Pr^i$)$_2Cl_4$(μ-H)(μ-PPh_2)] **6a** with estimated standard deviations (e.s.d.s) in parentheses. $Cp_{cent(1)}$ and $Cp_{cent(2)}$ refer to the computed η-$C_5H_4Pr^i$ ring centroids for W(1) and W(2) respectively

W(1)–W(2)	2.6558(3)	W(1)–Cl(1)	2.424(2)
W(1)–Cl(2)	2.410(2)	W(1)–P	2.388(2)
W(2)–Cl(3)	2.433(2)	W(2)–Cl(4)	2.400(2)
W(2)–P	2.398(1)	P–C(17)	1.825(6)
P–C(23)	1.829(6)	W(1)–$Cp_{cent(1)}$	2.020
W(2)–$Cp_{cent(2)}$	2.018		
Cl(1)–W(1)–W(2)	126.01(4)	Cl(2)–W(1)–W(2)	99.57(4)
Cl(2)–W(1)–Cl(1)	81.55(6)	P–W(1)–W(2)	56.47(3)
P–W(1)–Cl(1)	82.22(5)	P–W(1)–Cl(2)	131.07(6)
Cl(3)–W(2)–W(1)	127.12(4)	Cl(4)–W(2)–W(1)	99.50(4)
Cl(4)–W(2)–Cl(3)	81.16(6)	P–W(2)–W(1)	56.11(4)
P–W(2)–Cl(3)	82.94(5)	P–W(2)–Cl(4)	129.86(6)
W(2)–P–W(1)	67.42(4)	C(17)–P–W(1)	115.1(2)
C(17)–P–W(2)	129.0(2)	C(23)–P–W(1)	128.3(2)
C(23)–P–W(2)	117.9(2)	C(23)–P–C(17)	99.9(3)
W(2)–W(1)–$Cp_{cent(1)}$	120.1	W(1)–W(2)–$Cp_{cent(2)}$	118.5
P–W(1)–$Cp_{cent(1)}$	115.7	P–W(2)–$Cp_{cent(2)}$	115.7
Cl(1)–W(1)–$Cp_{cent(1)}$	107.6	Cl(2)–W(1)–$Cp_{cent(1)}$	113.2
Cl(3)–W(2)–$Cp_{cent(2)}$	108.3	Cl(4)–W(2)–$Cp_{cent(2)}$	114.4

induced addition of H_2 to [Mo_2(η-C_5Me_5)$_2$(CO)$_4$] has been described.[8] Compound **3** may be considered as another model for a mode of chemisorption of H_2 at a metal surface.

Reaction with HCl.—When HCl gas was passed through a toluene solution of [W_2(η-C_5H_4R)$_2Cl_4$] (R = Pr^i, **1a**; or Me, **1b**) a red colour was observed and the μ-chloro complexes [W_2(η-C_5H_4R)$_2Cl_4$(μ-Cl)(μ-H)] (R = Pr^i, **5a**; or Me, **5b**) were obtained in high yield on subsequent crystallisation. The room-temperature ^{1}H and ^{13}C NMR spectra of **5** showed resonances assignable to a single η-C_5H_4R moiety. In the ^{1}H NMR spectrum the ring protons appeared as a pair of mutually coupled AA′BB′ virtual triplets. An additional resonance at higher field with relative integration of one proton per two η-C_5H_4R rings and which possessed ^{183}W satellites consistent with a W(μ-H)W moiety was assigned as a briding hydride ligand. The compounds **5** are fluxional at room temperature since the NMR spectra of cold (−30 to −70 °C) [$^2H_2$]dichloromethane solutions show resonances assignable to a diastereotopic η-C_5H_4R ligand (Table 1). Thus in the slow-exchange limit the ring protons of **5** appear as mutually coupled ABCD virtual quartets. The chemical shift and coupling to ^{183}W of the μ-hydride ligand are essentially unaffected on passing from the fast- to the slow-exchange limiting spectra. On the basis of these data we propose that the compounds **5** have the structure shown in Scheme 1, although from the spectroscopic data alone we cannot rule out an alternative structure with a *cis* disposition of the η-C_5H_4R ligands.

The $\Delta G^‡$ values for the fluxional process in complexes **5a** and **5b** have been determined from ^{1}H NMR coalescence studies. For uncoupled, adiabatic, two-site exchange, $\Delta G^‡$ at coalescence is obtained from equation (1) where T_c is the coalescence

$$\Delta G^‡ = 4.573T_c[9.972 \log_{10}(T_c/\delta\nu)] \quad (1)$$

temperature and δν is the frequency separation of the two resonances in the low-temperature (slow-exchange) limit.[9] For **5a** and **5b** the measured values of $\Delta G^‡$ (coalescence temperature) are 12.5 ± 0.15 (263 K) and 12.3 ± 0.15 (268 K) kcal mol^{-1} respectively.

One possible mechanism for the exchange process in compounds **5** is shown in Fig. 1 and effectively involves rotation of the (μ-Cl)(μ-H) moiety about the W–W vector. If the η-C_5H_4R ligand is considered to occupy a single co-ordination site and the W–W bond is ignored then the process may be described as the interconversion between edge-sharing square-based pyramidal and trigonal-bipyramidal isomers. The geometry of the proposed trigonal-bipyramidal intermediate belongs to the point group C_s and thus accounts for the ABCD ⟶ AA′BB′ appearance of the η-C_5H_4R ligands in the NMR spectra on passing from the slow- to the fast-exchange limit. The mechanism illustrated in Fig. 1 is analogous to that proposed by other workers for enantiomer conversion in the μ-phosphido carbonyl complexes [Mo_2(η-C_5H_5)$_2$(CO)$_4$(μ-H)(μ-PPhR)] (R = H or Ph).[10]

Reactions with Primary or Secondary Phosphines.—The compounds **1** and **2** readily add to the P–H bond of $PHPh_2$ to afford the corresponding red-brown μ-phosphido complexes [W_2(η-C_5H_4R)$_2X_4$(μ-H)(μ-PPh_2)] (X = Cl, R = Pr^i **6a** or Me **6b**; X = Br, R = Pr^i **7**) which were characterised by elemental analysis and by ^{1}H and ^{31}P NMR spectroscpy (Table 1). For the compounds **6** ^{13}C NMR data were also recorded, and a single-crystal X-ray diffraction analysis was performed for **6a**. The molecular structure is shown in Fig. 2, selected bond lengths and angles are listed in Table 2, and fractional atomic co-ordinates for the non-hydrogen atoms are given in Table 3.

The molecular structure of **6a** possesses C_2 symmetry and consists of a W_2(η-$C_5H_4Pr^i$)$_2Cl_4$ unit in a staggered, *anti* conformation and with the W–W vector bridged by PPh_2 and H ligands. The μ-H ligand could not be located from a Fourier difference synthesis, but its position may be inferred from the vacant site *trans* to the μ-P atom and from the ^{1}H NMR spectra for **6** and **7** (see below). The W–W bond length in **6a** [2.6558(3) Å] is substantially lengthened from that found for its tungsten–tungsten triply bonded precursor **1a** [W≡W 2.3678(6) Å] [1] consistent with a reduced metal–metal bond order. Simple electron-counting procedures and a qualitative molecular-orbital interpretation of the metal–metal bonding in **6a** suggest a formal W=W double bond of electronic configuration $\sigma^2\pi^2$.

A large degree of steric congestion associated with the bulky

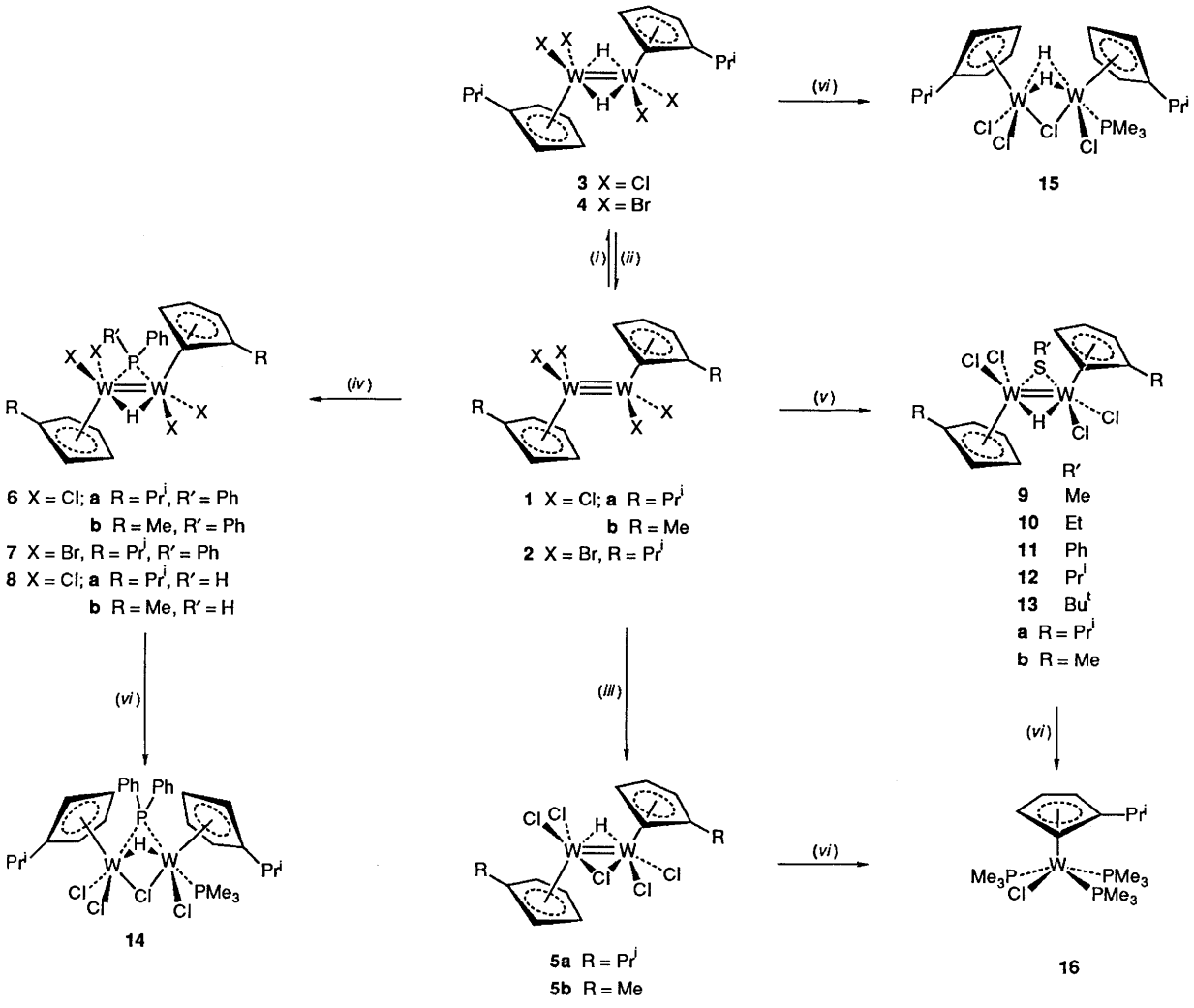

Scheme 1 Reagents: (*i*) H_2, 3 atm, 2 h, yield *ca.* 100%; (*ii*) (for X = Cl only) 50 °C, [$^2H_8$]toluene, 100% (according to ^1H NMR spectroscopy); (*iii*) HCl, toluene, 5 min, >90%; (*iv*) PHPhR′ (R′ = H or Ph), toluene, 12 h, >80%; (*v*) R′SH, toluene, 5 (R′ = Me) or 30 min (R′ = Bu^t) or 12 h (R′ = Et, Ph or Pr^i), >70%; (*vi*) excess of PMe_3, toluene, *ca.* 45%

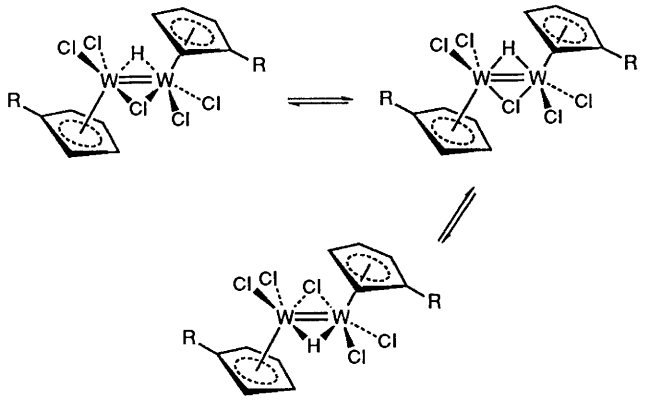

Fig. 1 Possible fluxional process for $[W_2(\eta\text{-}C_5H_4R)_2Cl_4(\mu\text{-}Cl)(\mu\text{-}H)]$ (R = Pr^i, **5a**; or Me, **5b**)

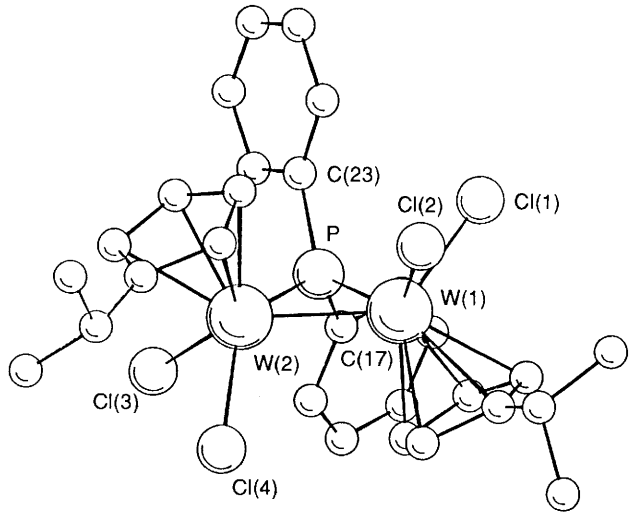

Fig. 2 Molecular structure of $[W_2(\eta\text{-}C_5H_4Pr^i)_2Cl_4(\mu\text{-}H)(\mu\text{-}PPh_2)]$ **6a**. Hydrogen atoms omitted for clarity

μ-PPh_2 linkage is indicated by substantial differences between the W–W–Cl angles for the Cl ligands *cis* to the μ-PPh_2 unit [W–W–Cl (average) 126.8°] and those *trans* to it [W–W–Cl (average) 99.4°]. For comparison, the average W–W–Cl angle found for complex **1a**, in which all the W–W–Cl values are equivalent within their associated estimated errors, is 100.3°.[1] The molecular structure of **6a** may be compared to that of $[Mo_2(\eta\text{-}C_5H_5)_2(CO)_3\{P(OMe)_3\}(\mu\text{-}H)(\mu\text{-}PPh_2)]$.[10] The latter possesses a *trans* disposition of the η-C_5H_5 ligands and has a comparable mean M–(μ-P) bond length, but a significantly longer metal–metal bond [Mo–Mo 3.254(1) Å] and larger M–(μ-P)–M angle [Mo–(μ-P)–Mo 84.2(1)° as compared to W(1)–P–W(2) 67.55(9) Å for **6a**]. The related complex $[W_2(\eta\text{-}C_5H_5)_2(CO)_4(\mu\text{-}H)(\mu\text{-}PH_2)]$ has also been described but no structural data are available.[11]

Table 3 Fractional atomic coordinates for $[W_2(\eta\text{-}C_5H_4Pr^i)_2Cl_4(\mu\text{-}H)(\mu\text{-}PPh_2)]$ **6a** with e.s.d.s in parentheses

Atom	*X/a*	*Y/b*	*Z/c*
W(1)	0.112 877(7)	0.429 88(2)	0.673 62(1)
W(2)	0.180 960(7)	0.536 55(2)	0.599 57(1)
Cl(1)	0.030 28(5)	0.458 9(2)	0.653 4(1)
Cl(2)	0.098 97(6)	0.277 5(1)	0.583 1(1)
Cl(3)	0.221 16(6)	0.707 7(1)	0.641 1(1)
Cl(4)	0.246 75(5)	0.450 6(1)	0.662 4(1)
P	0.114 89(5)	0.630 2(1)	0.654 94(8)
C(1)	0.116 3(2)	0.277 0(6)	0.769 8(4)
C(2)	0.082 4(2)	0.355 3(6)	0.794 0(4)
C(3)	0.103 6(3)	0.462 1(6)	0.804 5(4)
C(4)	0.151 5(3)	0.451 6(6)	0.788 5(4)
C(5)	0.158 9(2)	0.339 7(6)	0.764 8(4)
C(6)	0.112 1(3)	0.152 7(6)	0.755 8(5)
C(7)	0.061 9(3)	0.114 5(8)	0.750 3(6)
C(8)	0.137 8(4)	0.091 3(9)	0.821 0(9)
C(9)	0.221 6(2)	0.489 1(6)	0.478 0(3)
C(10)	0.209 5(2)	0.604 8(6)	0.474 2(4)
C(11)	0.160 8(2)	0.616 4(6)	0.482 2(4)
C(12)	0.141 4(2)	0.507 1(7)	0.487 2(3)
C(13)	0.178 7(2)	0.430 2(6)	0.487 8(4)
C(14)	0.268 3(2)	0.435 2(6)	0.467 0(4)
C(15)	0.308 0(3)	0.517 4(8)	0.480 8(6)
C(16)	0.270 6(3)	0.379(1)	0.388 1(6)
C(17)	0.111 4(2)	0.714 2(5)	0.743 9(3)
C(18)	0.148 6(2)	0.743 9(5)	0.791 9(4)
C(19)	0.140 1(3)	0.794 4(6)	0.862 7(4)
C(20)	0.095 9(3)	0.815 4(6)	0.887 8(4)
C(21)	0.058 9(3)	0.787 2(7)	0.840 6(4)
C(22)	0.066 4(2)	0.737 2(6)	0.769 4(4)
C(23)	0.078 6(2)	0.716 6(5)	0.590 4(3)
C(24)	0.085 4(2)	0 832 1(6)	0.593 9(4)
C(25)	0.062 4(3)	0.905 1(7)	0.541 3(5)
C(26)	0.032 7(3)	0.860 8(7)	0.488 4(5)
C(27)	0.025 4(2)	0.746 2(8)	0.483 2(4)
C(28)	0.048 2(2)	0.672 8(6)	0.534 5(4)

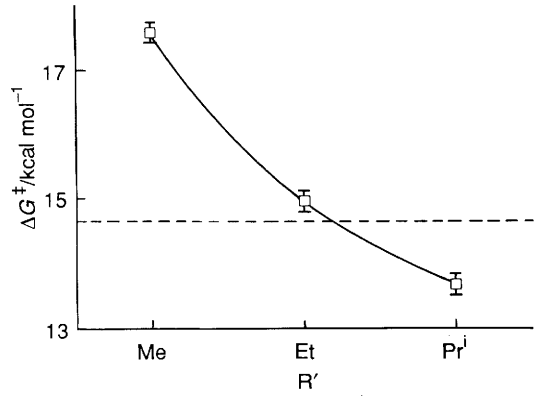

Fig. 3 Plot of $\Delta G^{\ddagger}$ against R′ group for the fluxional process in $[W_2(\eta\text{-}C_5H_4Pr^i)_2Cl_4(\mu\text{-}H)(\mu\text{-}SR')]$ [R′ = Me, **9a**; Et, **10a**; or Pr^i, **12a**]. The value for **11a** (R′ = Ph) is indicated by the horizontal dashed line. All data have been normalised to 320 K; the line joining the data points for **9a**, **10a** and **12a** was fitted by simple interpolation

The solution NMR spectra for complexes **6** and **7** are consistent with the maintenance of the geometry found in the solid state for **6a**. The $\eta\text{-}C_5H_4R$ ligands are diastereotopic and the μ-H and μ-P atoms show coupling to ^{183}W that is consistent with a $W(\mu\text{-}H)(\mu\text{-}PPh_2)W$ unit (Table 1). The μ-hydride ligand shows additional coupling [$^2J(^1H\text{–}^{31}P) \approx 6$ Hz] to the phosphorus nucleus of the $\mu\text{-}PPh_2$ linkage.

In a similar manner to that described above for $PHPh_2$, toluene solutions of complex **1** react with the primary phosphine PH_2Ph to give the μ-phosphido derivatives $[W_2(\eta\text{-}C_5H_4R)_2Cl_4(\mu\text{-}H)(\mu\text{-}PHPh)]$ (R = Pr^i, **8a**; or Me, **8b**) in high yields. Compounds **8** were characterised by elemental analysis and by ^1H, ^{13}C and ^{31}P NMR spectroscopy. The NMR spectra for **8** are largely analogous to those described above for **6** and **7** but show important differences. For **8** there are two inequivalent, diastereotopic $\eta\text{-}C_5H_4R$ ligands (proximal to either the PH or PPh functionality), and the μ-H and μ-P ligands show slightly different coupling constants for the two ^{183}W nuclei. In the ^1H NMR spectrum an additional doublet [$^1J(^1H\text{–}^{31}P) \approx 430$ Hz] at *ca.* δ 10.6 which integrates as one proton per molecule of **8** is assigned to the P–H proton. The proposed structure of **8** is illustrated in Scheme 1.

We were interested to see if the μ-phosphido complexes described above would exhibit fluxional behaviour similar to that found for the μ-chloro dimers **5** and the analogous dimolybdenum carbonyl species $[Mo_2(\eta\text{-}C_5H_5)(CO)_4(\mu\text{-}H)(\mu\text{-}PPhR)]$ (R = H or Ph) mentioned above.[10] However, heating a [$^2H_8$]toluene solution of **6b** or **7a** at 95 °C showed no evidence for fluxionality in the ^1H NMR spectra. This contrasts with the dynamic behaviour of the μ-chloro or dimolybdenum carbonyl species for which the onset of fluxionality is at *ca.* −50 to −30 °C. One rationalisation of these observations may be the substantially shorter metal–metal bond length in the ditungsten complexes as compared to that of the dimolybdenum μ-phosphido species. This could clearly lead to a greater steric barrier to rotation for complexes of the type $[W_2(\eta\text{-}C_5H_4R)_2X_4(\mu\text{-}H)(\mu\text{-}PPhR')]$ than for $[Mo_2(\eta\text{-}C_5H_5)(CO)_4(\mu\text{-}H)(\mu\text{-}PPhR)]$. For the μ-chloro complex **5**, the smaller steric requirement of Cl as compared to that of PPhR could account for its fluxionality. However, it is also possible that more subtle electronic factors arising from the presence of the lone pair of the μ-chloro ligand may be important.

Reactions with Alkane- and Arene-thiols.—Since the W≡W bond in complex **1** undergoes oxidative-addition reactions with P–H and Cl–H bonds, we were interested to investigate the reactions of **1** with thiols. Thus treatment of toluene solutions of $[W_2(\eta\text{-}C_5H_4R)_2Cl_4]$ with an excess of R′SH afforded the corresponding red-brown μ-thiolato derivatives $[W_2(\eta\text{-}C_5H_4R)_2Cl_4(\mu\text{-}H)(\mu\text{-}SR')]$ (R′ = Me **9**, Et **10**, Ph **11**, Pr^i **12** or Bu^t **13**; R = Pr^i **a** or Me **b**) in good yields. Compounds **9**–**13** are fluxional. The slow-exchange limit for **13** and the fast-exchange limit for **9** could not be observed on the NMR time-scale over the temperature range studied (−80 to +95 °C). For compounds **9**–**12** the low-temperature spectra featured two diastereotopic $\eta\text{-}C_5H_4R$ ring environments. For **10** and **12** the μ-SR′ linkages are diastereotopic, and the ^1H NMR spectra show a high-field resonance integrating as one proton and exhibiting coupling to ^{183}W indicative of a W(μ-H)W unit. These data are consistent with the structure shown in Scheme 1 for $[W_2(\eta\text{-}C_5H_4R)_2Cl_4(\mu\text{-}H)(\mu\text{-}SR')]$. The NMR spectra complexes of **10**–**13** in the fast-exchange limit are largely similar to those described for the slow-exchange limit except that only one type of diastereotopic $\eta\text{-}C_5H_4R$ ligand was observed. The μ-SR′ linkages of **10** (R′ = Et) and **12** (R′ = Pr^i) remained diastereotopic. Negligible changes were observed in either the chemical shift or the magnitude of coupling to ^{183}W of the μ-H ligand, with the exception of **11a** (R = Pr^i, R′ = Ph), in which the μ-H ligand does not couple equally to the two ^{183}W nuclei in the slow-exchange limit but possesses only one resolvable coupling constant in the fast-exchange limit. It is noted that the μ-H ligand of $[W_2(\eta\text{-}C_5H_4R)_2Cl_4(\mu\text{-}H)(\mu\text{-}PHPh)]$ **8** also showed two resolvable coupling constants to ^{183}W, while for the $\mu\text{-}PPh_2$ analogues **6** (in which the two W atoms are related by a molecular C_2 axis) only one set of satellites could be resolved.

Investigation of the Fluxional Process in $[W_2(\mu\text{-}C_5H_4R)_2Cl_4(\mu\text{-}H)(\mu\text{-}SR')]$.—To probe further the nature of the fluxional process for the μ-thiolato complexes, we measured the free energy of activation for the $\eta\text{-}C_5H_4Pr^i$ ring-exchange process for the four complexes **9a**, **10a**, **11a** and **12a**. Details of the

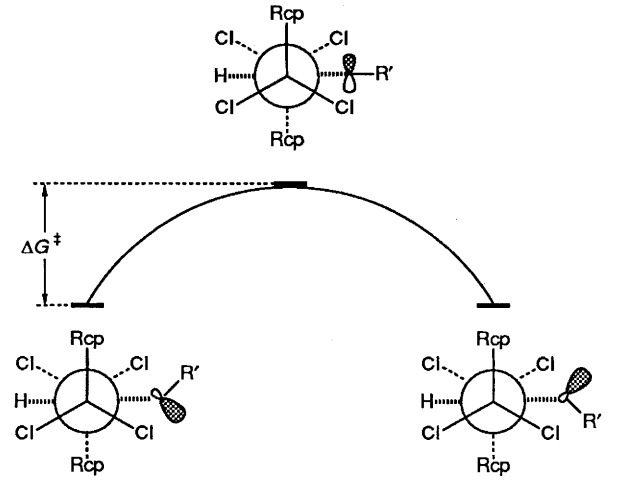

Fig. 4 Proposed fluxional process for $[W_2(\eta\text{-}C_5H_4R)_2Cl_4(\mu\text{-}H)(\mu\text{-}SR')]$ (R′ = Me **9**, Et **10**, Ph **11**, Pr^i **12** or Bu^t **13**; R = Pr^i **a** or Me **b**). The molecule is viewed as a Newman projection along the W–W vector with Rcp representing $\eta\text{-}C_5H_4R$. At left and right are the proposed ground-state structures (tetrahedral geometry at S); at centre is shown the intermediate geometry (trigonal geometry at S)

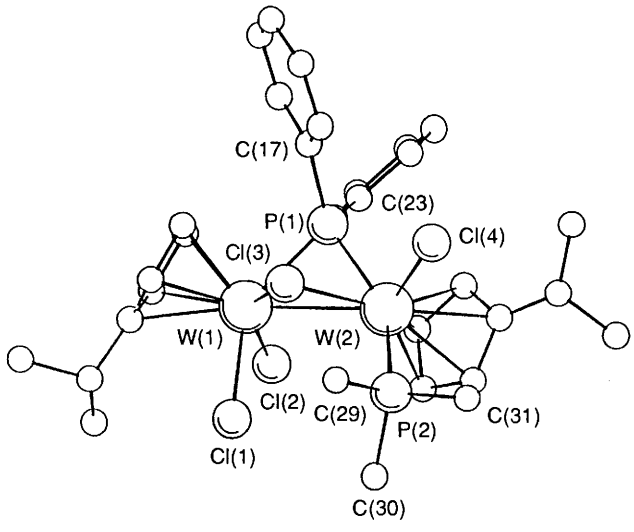

Fig. 5 Molecular structure of $[W_2(\eta\text{-}C_5H_4Pr^i)_2Cl_3(\mu\text{-}Cl)(\mu\text{-}H)(\mu\text{-}PPh_2)(PMe_3)]$ **14**. Hydrogen atoms omitted for clarity

measurements are given in the Experimental section. The results are shown in Fig. 3 where $\Delta G^{\ddagger}$ (normalised to 320 K) is plotted against the R′ group (Me, Et or Pr^i). The value for R′ = Ph is indicated by the horizontal dashed line. Fig. 3 shows that $\Delta G^{\ddagger}$ decreases with increasing steric bulk of the μ-SR′ moiety, with μ-SPh being intermediate in steric demand between that of the μ-SEt and -SPr^i linkages. As mentioned above, decoalescence for the μ-SBu^t homologue could not be observed in either the ^1H or ^{13}C NMR spectra at −80 °C.

A mechanism analogous to that proposed for the μ-chloro complexes **5** [*i.e.* rotation of the (μ-H)(μ-SR′) moiety about the W–W vector] is unlikely to account for the ring-exchange process since the μ-phosphido complex $[W_2(\eta\text{-}C_5H_4Pr^i)_2Cl_4(\mu\text{-}H)(\mu\text{-}PHPh)]$ **8a** is static on the NMR time-scale to at least 90 °C, whereas the μ-SPh analogues **11** show the onset of fluxional behaviour at 30 °C. Instead we propose a mechanism involving lone-pair inversion at the μ-S atom (as illustrated in Fig. 4) to account for both the $\eta\text{-}C_5H_4R$ ring-exchange process and the dependency of $\Delta G^{\ddagger}$ on the steric demands of μ-SR′. The electronic barrier to lone-pair inversion for pyramidal molecules of the type AX_3(lone pair) is well understood;[12] the dynamic behaviour of metal thiolato complexes has recently been reviewed, and the values of $\Delta G^{\ddagger}$ found for the complexes

Table 4 Selected bond lengths (Å) and angles (°) for $[W_2(\eta\text{-}C_5H_4Pr^i)_2Cl_3(\mu\text{-}Cl)(\mu\text{-}H)(\mu\text{-}PPh_2)(PMe_3)]\cdot CH_2Cl_2$ **14**·CH_2Cl_2 with e.s.d.s in parentheses. $Cp_{cent(1)}$ and $Cp_{cent(2)}$ refer to the computed $\eta\text{-}C_5H_4Pr^i$ ring centroids for W(1) and W(2) respectively

W(1)–W(2)	3.1165(2)	W(1)–Cl(1)	2.493(1)
W(1)–Cl(2)	2.460(1)	W(1)–Cl(3)	2.471(1)
W(1)–P(1)	2.443(1)	W(2)–Cl(3)	2.501(1)
W(2)–Cl(4)	2.482(1)	W(2)–P(1)	2.524(1)
W(2)–P(2)	2.565(1)	P(1)–C(17)	1.842(5)
P(1)–C(23)	1.837(5)	P(2)–C(29)	1.811(6)
P(2)–C(30)	1.816(6)	P(2)–C(31)	1.827(6)
W(1)–$Cp_{cent(1)}$	1.96	W(2)–$Cp_{cent(2)}$	1.98
Cl(5)–C(32)	1.72(1)*	Cl(6)–C(32)	1.73(1)*
Cl(1)–W(1)–W(2)	88.59(3)	Cl(2)–W(1)–W(2)	94.17(3)
Cl(2)–W(1)–Cl(1)	82.68(5)	Cl(3)–W(1)–W(2)	51.62(3)
Cl(3)–W(1)–Cl(1)	84.18(4)	Cl(3)–W(1)–Cl(2)	143.57(4)
P(1)–W(1)–W(2)	52.31(3)	P(1)–W(1)–Cl(1)	140.80(4)
P(1)–W(1)–Cl(2)	96.09(4)	P(1)–W(1)–Cl(3)	73.76(4)
Cl(3)–W(2)–W(1)	50.75(3)	P(2)–W(2)–P(1)	150.83(4)
Cl(4)–W(2)–W(1)	126.41(3)	Cl(4)–W(2)–Cl(3)	80.59(4)
P(1)–W(2)–W(1)	49.98(3)	P(1)–W(2)–Cl(3)	71.86(4)
P(1)–W(2)–Cl(4)	99.34(4)	P(2)–W(2)–W(1)	107.28(3)
P(2)–W(2)–Cl(3)	79.27(4)	P(2)–W(2)–Cl(4)	79.62(5)
W(2)–Cl(3)–W(1)	77.63(3)	W(2)–P(1)–W(1)	77.71(3)
C(17)–P(1)–W(1)	117.0(2)	C(17)–P(1)–W(2)	123.8(2)
C(23)–P(1)–W(1)	123.3(2)	C(23)–P(1)–W(2)	119.7(2)
C(23)–P(1)–C(17)	97.4(2)	C(29)–P(2)–W(2)	116.4(2)
C(30)–P(2)–W(2)	115.2(2)	C(30)–P(2)–C(29)	102.8(3)
C(31)–P(2)–W(2)	116.4(2)	C(31)–P(2)–C(29)	100.1(3)
C(31)–P(2)–C(30)	103.9(3)	W(2)–W(1)–$Cp_{cent(1)}$	155.2
W(1)–W(2)–$Cp_{cent(2)}$	118.1	P(1)–W(1)–$Cp_{cent(1)}$	109.1
P(1)–W(2)–$Cp_{cent(2)}$	105.1	Cl(1)–W(1)–$Cp_{cent(1)}$	107.9
Cl(2)–W(1)–$Cp_{cent(1)}$	105.8	Cl(4)–W(2)–$Cp_{cent(2)}$	111.5
Cl(3)–W(2)–$Cp_{cent(2)}$	167.9		
Cl(6)–C(32)–Cl(5)	111.1(6)*		

* Value for the dichloromethane molecule of crystallisation.

9a–**12a** are comparable to those reported previously for other thiolato complexes.[13]

In the complexes under study here, the electronic contribution to $\Delta G^{\ddagger}$ may be assumed to be virtually independent of the nature or R′ (with the possible exception of R′ = Ph), but the contribution from the steric demands of R′ to $\Delta G^{\ddagger}$ will clearly depend on the size of R′. With sulphur in a pyramidal geometry (at left or right in Fig. 4) the R′ group is partially directed towards the proximal $\eta\text{-}C_5H_4R$ and Cl ligands, whereas for sulphur in a trigonal geometry (at centre in Fig. 4) the R′ group is orientated directly away from the other ligands. Therefore as R′ increases in bulk, the ground (pyramidal geometry) state will be destabilised relative to the excited (trigonal geometry) state, accounting for the observed trends in $\Delta G^{\ddagger}$ with the steric bulk of R′.

Reactions of $[W_2(\mu\text{-}C_5H_4Pr^i)_2Cl_4(\mu\text{-}H)(\mu\text{-}X)]$ (X = H, Cl, PPh_2 *or* SR′) *with* PMe_3.—The compound $[W_2(\eta\text{-}C_5H_4Pr^i)_2Cl_4(\mu\text{-}H)(\mu\text{-}PPh_2)]$ **6a** reacts with an excess of PMe_3 in toluene to give dark red microcrystals of the Lewis-base adduct $[W_2(\eta\text{-}C_5H_4Pr^i)_2Cl_3(\mu\text{-}Cl)(\mu\text{-}H)(\mu\text{-}PPh_2)(PMe_3)]$ **14** in good yield. Compound **14** was characterised by elemental analysis, and by ^1H, ^{31}P and ^{13}C NMR spectroscopy (Table 1). Single crystals of **14**·CH_2Cl_2 suitable for an X-ray diffraction analysis were obtained from a concentrated dichloromethane solution. The molecular structure of **14** is shown in Fig. 5, selected bond lengths and angles are listed in Table 4, and fractional atomic coordinates for the non-H atoms are given in Table 5.

The molecular structure of complex **14** consists of the fragments $W(\eta\text{-}C_5H_4Pr^i)Cl_2$ and $W(\eta\text{-}C_5H_4Pr^i)Cl(PMe_3)$ joined by bridging Cl, H and PPh_2 ligands. The μ-hydrido ligand could not be located from a Fourier difference synthesis,

Table 5 Fractional atomic coordinates for $[W_2(\eta\text{-}C_5H_4Pr^i)_2Cl_3(\mu\text{-}Cl)(\mu\text{-}H)(\mu\text{-}PPh_2)(PMe_3)]\cdot CH_2Cl_2$ **14**·CH_2Cl_2 with e.s.d.s in parentheses

Atom	*X/a*	*Y/b*	*Z/c*	Atom	*X/a*	*Y/b*	*Z/c*
W(1)	0.164 06(2)	0.464 95(1)	0.237 06(1)	C(12)	0.051 6(5)	0.295 7(5)	0.160 8(4)
W(2)	−0.064 39(2)	0.369 23(1)	0.297 20(1)	C(13)	−0.003 2(5)	0.215 4(4)	0.242 8(4)
Cl(1)	0.022 21(1)	0.645 1(1)	0.151 6(1)	C(14)	−0.238 8(6)	0.191 8(5)	0.330 6(5)
Cl(2)	0.252 9(1)	0.442 7(1)	0.056 9(1)	C(15)	−0.299 4(6)	0.175 4(6)	0.261 1(6)
Cl(3)	−0.033 9(1)	0.473 7(1)	0.390 41(9)	C(16)	−0.174 8(9)	0.082 7(6)	0.398 7(6)
Cl(4)	−0.197 9(1)	0.303 4(1)	0.478 1(1)	C(17)	0.196 3(5)	0.217 0(4)	0.457 3(4)
Cl(5)	0.033 4(3)	0.001 4(2)	0.121 9(3)	C(18)	0.326 7(6)	0.162 2(4)	0.465 2(5)
Cl(6)	0.239 6(4)	0.098 7(3)	0.012 1(4)	C(19)	0.354 8(6)	0.123 0(5)	0.562 5(6)
P(1)	0.164 9(1)	0.276 0(1)	0.326 2(1)	C(20)	0.254 2(8)	0.136 3(5)	0.652 2(5)
P(2)	−0.281 9(1)	0.530 1(1)	0.302 3(1)	C(21)	0.125 8(7)	0.189 1(5)	0.646 3(5)
C(1)	0.286 0(5)	0.585 1(4)	0.207 5(4)	C(22)	0.095 3(6)	0.229 3(4)	0.550 0(4)
C(2)	0.214 2(5)	0.550 4(4)	0.314 4(4)	C(23)	0.279 5(5)	0.159 6(4)	0.270 8(4)
C(3)	0.268 2(5)	0.434 4(4)	0.350 8(4)	C(24)	0.383 4(6)	0.167 8(4)	0.180 5(5)
C(4)	0.368 0(5)	0.395 6(4)	0.264 2(5)	C(25)	0.471 5(7)	0.075 6(6)	0.146 0(6)
C(5)	0.378 4(5)	0.489 6(5)	0.177 7(5)	C(26)	0.454 7(7)	−0.025 7(5)	0.201 5(7)
C(6)	0.269 0(5)	0.700 8(3)	0.143 4(5)	C(27)	0.350 7(7)	−0.035 1(5)	0.289 5(6)
C(7)	0.325 3(9)	0.710 4(7)	0.025 5(6)	C(28)	0.264 5(6)	0.055 7(4)	0.325 2(5)
C(8)	0.331 0(9)	0.752 6(6)	0.181 0(8)	C(29)	−0.322 0(6)	0.612 2(6)	0.389 8(6)
C(9)	−0.142 0(5)	0.253 9(4)	0.260 2(4)	C(30)	−0.292 6(6)	0.631 8(5)	0.177 0(5)
C(10)	−0.173 4(5)	0.359 5(4)	0.191 4(4)	C(31)	−0.434 9(6)	0.495 1(6)	0.348 4(5)
C(11)	−0.056 1(6)	0.386 9(4)	0.129 1(4)	C(32)	0.083(1)	0.104 5(9)	0.019 5(9)

but its position may be inferred from the solution spectroscopic data (see below) and from the apparently vacant co-ordination site *trans* to the $\eta\text{-}C_5H_4Pr^i$ ring of W(1) and to Cl(4). The overall structure may be described as a confacial bioctahedron if the $\eta\text{-}C_5H_4Pr^i$ ligands are each considered to occupy a single co-ordination site and any metal–metal bond is ignored. The $\mu\text{-}PPh_2$ and PMe_3 ligands are mutually *trans* with the consequence that the $\mu\text{-}PPh_2$ ligand binds more tightly to W(1) [W(1)–P(1) 2.443(1) Å] than to W(2) [W(2)–P(1) 2.524(1) Å], presumably reflecting the greater *trans* influence of PMe_3 as compared to Cl. The W–W bond length [W(1)–W(2) 3.1165(2) Å] is substantially longer than that of the precursor **6a** [W–W 2.6558(3) Å].

Application of the electron-counting formalism that a bridging hydride ligand may be treated as a 'three-electron donor'[14a] suggests that no metal–metal bond is required in order to achieve an valence electron count of 18 for each metal centre in complex **14**. However, it is clear from the relatively close approach of the two W atoms that some degree of metal–metal interaction exists, but it is not possible to partition this between direct (W–W) and indirect [W–(μ-H)–W] contributions. Such ambiguities are not unusual in polynuclear, ligand-bridged systems; similar difficulties are encountered with understanding molecules even as (apparently) simple as diborane.[14b]

The solution ^1H, ^{13}C and ^{31}P NMR data for complex **14** are consistent with the maintenance of the solid-state molecular structure in solution. The μ-hydride ligand appears as a doublet of doublets due to coupling to the two inequivalent ^{31}P nuclei. The ^{31}P NMR spectrum shows a pair of mutually coupled doublets. The magnitude of $^2J(^{31}P\text{–}^{31}P)$ (83 Hz) is consistent with a *trans* arrangement of the PMe_3 and $\mu\text{-}PPh_2$ ligands, and the ^{183}W satellite intensities for the two sets of resonances are consistent with the presence of both terminal and bridging phosphorus atoms.

Toluene solutions of the di-μ-dihydrido complex **3** also react with PMe_3 to give purple microcrystals of $[W_2(\eta\text{-}C_5H_4Pr^i)_2Cl_3(\mu\text{-}Cl)(\mu\text{-}H)_2(PMe_3)]$ **15** in reasonable yield. The analytical and spectroscopic data for **15** (Table 1) are consistent with the structure illustrated in Scheme 1. Thus the ^{31}P NMR spectrum shows a single resonance at δ −22.7 consistent with the presence of a co-ordinated PMe_3 ligand, and the ^1H and ^{13}C NMR spectra exhibit resonances assignable to a PMe_3 moiety and to two types of diastereotopic $\eta\text{-}C_5H_4Pr^i$ ligands. In addition, the ^1H NMR spectrum shows two mutually coupled doublets of doublets at δ 2.59 and δ −4.59 integrating as one proton each and which show coupling to two ^{183}W nuclei.

In contrast to the reactions of PMe_3 with **3** or **6a** to give rise to dinuclear complexes, treatment of toluene solutions of $[W_2(\eta\text{-}C_5H_4Pr^i)_2Cl_4(\mu\text{-}Cl)(\mu\text{-}H)]$ **5a** or $[W_2(\eta\text{-}C_5H_4Pr^i)_2Cl_4(\mu\text{-}H)(\mu\text{-}SR')]$ **9a**–**13a** with an excess of PMe_3 afforded the mononuclear complex $[W(\eta\text{-}C_5H_4Pr^i)Cl(PMe_3)_3]$ **16** in *ca.* 40% yield (Scheme 1). Addition of a single equivalent of PMe_3 gave only complex mixtures which also contained unreacted ditungsten complex. Compound **16** was characterised by elemental analysis, and by ^1H and ^{31}P NMR spectroscopy (Table 1), as well as by comparison with the previously reported parent complex $[W(\eta\text{-}C_5H_5)Cl(PMe_3)_3]$.[15]

Experimental

All manipulations of air- and moisture-sensitive materials were performed using either standard Schlenk-line techniques under an atmosphere of dinitrogen, which had been purified by passage over BASF catalyst and 4 Å molecular sieves, or in an inert-atmosphere dry-box containing dinitrogen. Solvents were pre-dried by standing over 4 Å molecular sieves and then distilled under an atmosphere of dinitrogen from phosphorus pentaoxide (dichloromethane), sodium (toluene), potassium–benzophenone [thf (tetrahydrofuran)] or sodium–potassium alloy (1:3 w/w) [light petroleum (b.p. 40–60 °C), diethyl ether]. Deuteriated solvents for NMR studies were stored in a Young's ampoule under an atmosphere of dinitrogen over sodium–potassium alloy ($[^2H_6]$benzene, $[^2H_8]$toluene) or molecular sieves ($[^2H_2]$dichloromethane).

Proton, ^{13}C and $^{31}P\text{-}\{^1H\}$ NMR spectra were recorded on a Brüker AM 300 spectrometer (^1H, 300; ^{13}C, 75.5; ^{31}P, 121.6 MHz), ^{13}C using a gated sequence to give nuclear Overhauser enhancement. Spectra were referenced internally using the residual protio solvent (^1H) and solvent (^{13}C) resonances relative to tetramethylsilane (δ = 0), or externally using trimethyl phosphate in $[^2H_2]$water (^{31}P). All chemical shifts are quoted in δ (ppm) and coupling constants are in Hz.

Elemental analyses were performed by the analytical department of this laboratory and are expressed as found (required) in % w/w. The compounds $[W_2(\eta\text{-}C_5H_4R)_2X_4]$ (X = Cl, R = Pr^i or Me; X = Br, R = Pr^i) were prepared as described previously.[1]

Preparations.—$[W_2(\eta\text{-}C_5H_4Pr^i)_2X_4(\mu\text{-}H)_2]$ (X = Cl, **3**; *or* Br, **4**). A solution of $[W_2(\eta\text{-}C_5H_4Pr^i)_2Cl_4]$ (0.11 g, 0.15 mmol) in toluene (10 cm^3) was treated with dihydrogen (*ca.* 3 atm) for 2 h to afford a turquoise solution and microcrystalline

Table 6 Crystallographic data and data collection and processing parameters for $[W_2(\eta\text{-}C_5H_4Pr^i)_2Cl_4(\mu\text{-}H)(\mu\text{-}PPh_2)]$ **6a** and $[W_2(\eta\text{-}C_5H_4Pr^i)_2Cl_3(\mu\text{-}Cl)(\mu\text{-}H)(\mu\text{-}PPh_2)(PMe_3)]\cdot CH_2Cl_2$ **14**·CH_2Cl_2[a]

	6a	**14**·CH_2Cl_2
Formula	$C_{28}H_{33}Cl_4PW_2$	$C_{31}H_{42}Cl_4P_2W_2\cdot CH_2Cl_2$
Formula weight	910.04	1071.07
Crystal size/mm	0.15 × 0.20 × 0.35	0.15 × 0.20 × 0.30
Colour	Red	Red-brown
Crystal system	Monoclinic	Triclinic
Space group	$C2/c$	$P\bar{1}$
a/Å	28.756(4)	11.493(3)
b/Å	11.807(1)	13.917(6)
c/Å	17.175(5)	14.241(9)
α/°	—	67.57(5)
β/°	90.19(2)	67.35(4)
γ/°	—	65.34(2)
U/Å^3	5831.5	1923.0
Z	8	2
D_c/g cm^{-3}	2.07	1.85
μ/cm^{-1}	84.99	66.33
$F(000)$	3448	1032
Scan angle/°	0.90 + 0.35 (tan θ)	0.85 + 0.35 (tan θ)
Zone	$+h, +k, \pm l$	$+h, \pm k, \pm l$
Absorption (minimum, maximum)	2.34, 19.54	2.06, 6.18
Total unique data collected	5108	6478
No. of observations [$I > 3\sigma(I)$]	4125	5122
No. of variables	317	380
Observations/variables	13.0	13.5
Weighting coefficients	13.8, −8.13, 10.7	13.9, −16.9, 10.7, −2.7
Largest residual peak in final difference map/e Å^{-3}	1.2	1.1
R(merg)	0.037	0.017
R[b]	0.029	0.023
R'[c]	0.035	0.026

[a] Details in common: Mo-Kα radiation (λ 0.710 69 Å); 2θ range 0–50°; ω–2θ scan mode; horizontal aperture 3.50 mm. Chebyshev weighting scheme. [b] $\Sigma(|F_o| - |F_c|)/\Sigma|F_o|$. [c] $[\Sigma w(|F_o| - |F_c|)^2/\Sigma w|F_o|^2]^{\frac{1}{2}}$.

precipitate. The volume was reduced to *ca.* 5 cm^3 and light petroleum (5 cm^3) added. The green-brown supernatant was decanted and the turquoise microcrystals of complex **3** washed with light petroleum (2 × 10 cm^3) and dried *in vacuo*. Yield: 100 mg (90%). The complex $[W_2(\eta\text{-}C_5H_4Pr^i)_2Br_4(\mu\text{-}H)_2]$ **4** was prepared in a similar manner (yield: 90%).

$[W_2(\eta\text{-}C_5H_4R)_2Cl_4(\mu\text{-}Cl)(\mu\text{-}H)]$ (R = Pr^i, **5a**; *or* Me **5b**). Hydrogen chloride gas was bubbled through a solution of $[W_2(\eta\text{-}C_5H_4Me)_2Cl_4]$ (200 mg, 0.3 mmol) in toluene (*ca.* 20 cm^3) for 5 min at room temperature (r.t.). Concentration of the red-brown solution and cooling to −20 °C afforded dark red microcrystals. Subsequent recrystallization from dichloromethane–diethyl ether afforded analytically pure $[W_2(\eta\text{-}C_5H_4Me)_2Cl_4(\mu\text{-}Cl)(\mu\text{-}H)]$ **5b**. Yield: 190 mg (90%). The complex $[W_2(\eta\text{-}C_5H_4Pr^i)_2Cl_4(\mu\text{-}Cl)(\mu\text{-}H)]$ **5a** was prepared in a similar manner but was recrystallised from toluene–light petroleum (yield 90%).

$[W_2(\eta\text{-}C_5H_4R)_2X_4(\mu\text{-}H)(\mu\text{-}PPh_2)]$ (X = Cl, R = Pr^i **6a** *or* Me **6b**; X = Br, R = Pr^i **7**) *and* $[W_2(\eta\text{-}C_5H_4R)_2Cl_4(\mu\text{-}H)(\mu\text{-}PHPh)]$ (R = Pr^i, **8a**; *or* Me, **8b**). A solution of $[W_2(\eta\text{-}C_5H_4Me)_2Cl_4]$ (200 mg, 0.3 mmol) in toluene (*ca.* 20 cm^3) was treated with an excess of diphenylphosphine (17 mg, 0.9 mmol) to give a brown solution and precipitate. After 12 h the supernatant was decanted, and the residual solid was washed with light petroleum (3 × 20 cm^3) to remove unreacted phosphine. Subsequent recrystallisation of the residues from dichloromethane–diethyl ether afforded $[W_2(\eta\text{-}C_5H_4Me)_2Cl_4(\mu\text{-}H)(\mu\text{-}PPh_2)]\cdot 0.5CH_2Cl_2$ **6b**·$0.5CH_2Cl_2$ as red-brown microcrystals. Yield: 270 mg (95%). A similar procedure was used to prepare **6a**, **7**, **8a** and **8b** in >80% yield; the $\eta\text{-}C_5H_4Pr^i$ complexes **6a**, **7** and **8a** were recrystallised from toluene–light petroleum.

$[W_2(\eta\text{-}C_5H_4R)_2Cl_4(\mu\text{-}H)(\mu\text{-}SMe)]$ (R = Pr^i, **9a**; *or* Me **9b**). Methanethiol was passed through a cold (−70 °C) solution of $[W_2(\eta\text{-}C_5H_4Me)_2Cl_4]$ (200 mg, 0.3 mmol) in toluene (*ca.* 20 cm^3) for 5 min to afford a red-brown solution and a small amount of brown solid. The mixture was warmed to room temperature and the supernatant decanted. Reduction in volume and addition of light petroleum afforded more brown solid. Analytically pure complex **9b** was obtained by recrystallisation of the initial brown solid from dichloromethane–diethyl ether. Yield: 190 mg (90%). The compound **9a** was prepared in a similar manner (yield 90%) but with recrystallisation from toluene.

$[W_2(\eta\text{-}C_5H_4R)_2Cl_4(\mu\text{-}H)(\mu\text{-}SR')]$ (R′ = Et **10**, Ph **11** *or* Pr^i **12**; R = Pr^i **a** *or* Me **b**). A typical experiment was as follows. An excess of R′SH (*ca.* 0.5 cm^3) was added to a solution of $[W_2(\eta\text{-}C_5H_4R)_2Cl_4]$ (0.3 mmol) in toluene (*ca.* 20 cm^3) and the mixture stirred for 12 h to give a red solution and a small quantity of red precipitate. The supernatant was decanted and the solid was washed with light petroleum (3 × 10 cm^3). A further crop of red crystals was obtained by concentration of the supernatant and addition of light petroleum, followed by recrystallisation of the combined residues from toluene (R = Pr^i) or dichloromethane–diethyl ether (R = Me). Yield of $[W_2(\eta\text{-}C_5H_4R)_2Cl_4(\mu\text{-}H)(\mu\text{-}SR')] > 70\%$.

$[W_2(\eta\text{-}C_5H_4R)_2Cl_4(\mu\text{-}H)(\mu\text{-}SBu^t)]$ (R = Pr^i, **13a**; *or* Me, **13b**). An excess of Bu^{t}SH (*ca.* 0.5 cm^3) was added to a solution of $[W_2(\eta\text{-}C_5H_4Me)_2Cl_4]$ (200 mg, 0.3 mmol) in toluene (*ca.* 20 cm^3) to afford a red solution after 30 min. Volatiles were removed under reduced pressure and the residues washed several times with light petroleum. Subsequent recrystallisation from toluene–light petroleum afforded analytically pure complex **13b**. Yield: 170 mg (75%). A similar procedure was used to prepare **13a** (yield: 80%).

$[W_2(\eta\text{-}C_5H_4Pr^i)_2Cl_3(\mu\text{-}Cl)(\mu\text{-}H)(\mu\text{-}PPh_2)(PMe_3)]$ **14**. A solution of $[W_2(\eta\text{-}C_5H_4Pr^i)_2Cl_4(\mu\text{-}Cl)(\mu\text{-}H)]$ **5a** (200 mg, 0.22 mmol) in toluene (*ca.* 30 cm^3) was treated with an excess of

PMe_3 (*ca.* 0.3 cm^3). After 12 h the volatiles were removed under reduced pressure. Recrystallisation from dichloromethane–light petroleum afforded the required compound as red microcrystals. Yield: 170 mg (70%).

$[W_2(\eta\text{-}C_5H_4Pr^i)_2Cl_3(\mu\text{-}Cl)(\mu\text{-}H)_2(PMe_3)]$ **15**. A solution of $[W_2(\eta\text{-}C_5H_4Pr^i)_2Cl_4(\mu\text{-}H)_2]$ **3** (0.25 g, 0.34 mmol) in toluene (10 cm^3) was treated with PMe_3 (0.21 g, 2.7 mmol) in toluene (6 cm^3) to give a purple-brown solution and a pale flocculent precipitate. After 2 h, the volatiles were removed under reduced pressure, the residues washed with light petroleum (10 cm^3) and diethyl ether (2 × 10 cm^3) and then extracted with toluene (2 × 10 cm^3). The purple toluene solution was filtered through Celite, reduced in volume to *ca.* 8–10 cm^3 and layered with light petroleum to give complex **15** as a purple solid which was washed with toluene (5 cm^3), light petroleum (2 × 5 cm^3), and dried *in vacuo*. Yield: 120 mg (44%).

$[W(\eta\text{-}C_5H_4Pr^i)Cl(PMe_3)_3]$ **16**. A solution of $[W_2(\eta\text{-}C_5H_4Pr^i)_2Cl_4(\mu\text{-}H)(\mu\text{-}Y)]$ (Y = Cl or SR′) (0.25 mmol) in toluene (*ca.* 30 cm^3) was treated with an excess of PMe_3 (*ca.* 0.5 cm^3) to give a pale yellow precipitate which was washed with light petroleum and dried *in vacuo*. Yield: *ca.* 45%.

Measurement of $\Delta G^{\ddagger}$ *for the Complexes* **9a**, **10a**, **11a** *and* **12a**.—The value of $\Delta G^{\ddagger}$ for complex **9a** was obtained using data from the two-dimensional ^1H PSEXY (phase-sensitive exchange correlation spectroscopy) experiment (standard Brüker software) and the D2DNMR program of Abel *et al.*[16] to obtain the rate constants for the $\eta\text{-}C_5H_4Pr^i$ ring-exchange process at three different temperatures. Subsequent fitting of the rate constants to the Arrhenius equation afforded E_a 21.7 ± 0.1 kcal mol^{-1} from which $\Delta H^{\ddagger}$ 21.1 ± 0.1 kcal mol^{-1}, $\Delta S^{\ddagger}$ 11.5 ± 2.5 cal K^{-1} mol^{-1} and $\Delta G^{\ddagger}$ 17.6 ± 0.2 kcal mol^{-1} (T = 320 K) were computed.[9] For **10a**, **11a** and **12a** the values of $\Delta G^{\ddagger}$ directly obtained from coalescence studies [using equation (1) above] were normalised to 320 K assuming $\Delta S^{\ddagger}$ to be approximately equal to that measured for **9a**.

X-Ray Crystal Structure Determination of Complexes **6a** *and* **14**.—Crystal data and data collection and processing parameters are given in Table 6. The general procedure was as follows. A crystal was sealed in a Lindemann glass capilliary and transferred to the goniometer head of an Enraf-Nonius CAD4-F diffractometer interfaced to a PDP 11/23 and LSI minicomputer. Unit-cell parameters were calculated from the setting angles of 25 carefully centred reflections. Three reflections were chosen as intensity standards and were measured every 3600 s of X-ray exposure time, and three orientation controls were measured every 250 reflections.

The data were corrected for Lorentz and polarisation effects and an empirical absorption correction[17] based on an azimuthal scan was applied. Equivalent reflections were merged and systematically absent reflections rejected. The tungsten atom positions were determined from a Patterson synthesis. Subsequent Fourier difference syntheses revealed the positions of other non-hydrogen atoms. The crystals of complex **14** contained one molecule of dichloromethane in each asymmetric unit. For **6a** a possible higher symmetry (*C*-centred orthorhombic) was eliminated by close examination of the $h\,k \pm l$ classes of reflection. Non-hydrogen atoms were refined with anisotropic thermal parameters by least-squares procedures and hydrogen atoms were placed in estimated positions (C–H 0.96 Å). A Chebyshev weighting scheme[18] was applied and the data were corrected for the effects of anomalous dispersion and isotropic extinction (*via* an overall isotropic extinction parameter[19]) in the final stages of refinement. All crystallographic calculations were performed using the CRYSTALS suite[20] on a micro VAX 3800 computer in the Chemical Crystallography Laboratory, Oxford. Scattering factors were taken from the usual sources.[21]

Additional material available for both structures from the Cambridge Crystallographic Data Centre comprises H-atom coordinates, thermal parameters and remaining bond lengths and angles.

Acknowledgements

We thank the Chinese Government and CIRIT Generalitat de Catalunya for support (to Q. F. and M. F.), Dr. E. W. Abel for a copy of the D2DNMR program, and Dr. A. K. Hughes for helpful discussion.

References

1 M. L. H. Green, J. D. Hubert and P. Mountford, *J. Chem. Soc., Dalton Trans.*, 1990, 3793.
2 M. L. H. Green and P. Mountford, *Organometallics*, 1990, **9**, 886.
3 J. C. Green, M. L. H. Green, P. Mountford and M. J. Parkington, *J. Chem. Soc., Dalton Trans.*, 1990, 3407.
4 M. H. Chisholm and I. P. Rothwell, *Prog. Inorg. Chem.*, 1982, **29**, 1; L. Messerle, *Chem. Rev.*, 1988, **88**, 1229; M. J. Winter, *Adv. Organomet. Chem.*, 1989, **29**, 101.
5 M. L. H. Green and P. Mountford, *J. Chem. Soc., Chem. Commun.*, 1989, 732.
6 G. A. Kubas, *Comments Inorg. Chem.*, 1988, **7**, 17.
7 Unpublished work cited in W. A. Herrmann, *Angew. Chem., Int. Ed. Engl.*, 1988, **27**, 1297.
8 H. G. Alt, K. A. Mahmood and A. J. Rest, *Angew. Chem., Int. Ed. Engl.*, 1983, **22**, 544.
9 J. Sandström, *Dynamic NMR Spectroscopy*, Academic Press, London, 1982.
10 K. Henrick, M. McPartlin, A. D. Horton and M. J. Mays, *J. Chem. Soc., Dalton Trans.*, 1988, 1083.
11 E. A. V. Ebsworth, A. P. McIntosh and M. Schröder, *J. Organomet. Chem.*, 1986, **312**, C41.
12 T. A. Albright, J. K. Burdett and M.-H. Whangbo, *Orbital Interactions in Chemistry*, Wiley-Interscience, New York, 1985, p. 143.
13 E. W. Abel, K. G. Orell and S. K. Bhargava, *Prog. Inorg. Chem.*, 1984, **32**, 1.
14 (*a*) M. Berry, N. J. Cooper, M. L. H. Green and S. J. Simpson, *J. Chem. Soc., Dalton Trans.*, 1980, 29; (*b*) W. N. Lipscomb, in *Boron Hydride Chemistry*, ed. E. L. Muetterties, Academic Press, New York, 1975, p. 39; *Boron Hydrides*, W. A. Benjamin, New York, 1963; E. A. Laws, R. M. Stevens and W. N. Lipscomb, *J. Am. Chem. Soc.*, 1972, **94**, 4461.
15 D. K. Siriwardene, D. Phil. Thesis, Oxford, 1987.
16 E. W. Abel, T. P. J. Coston, K. G. Orrell, V. Sik and D. Stephenson, *J. Magn. Reson.*, 1986, **70**, 34.
17 A. C. T. North, D. C. Philips and F. S. Mathews, *Acta Crystallogr., Sect. A*, 1968, **24**, 351.
18 J. S. Rollet, *Computing Methods in Crystallography*, Pergamon, Oxford, 1965.
19 A. C. Larson, *Acta Crystallogr., Sect. A*, 1967, **23**, 664.
20 D. J. Watkin, J. R. Carruthers and P. W. Betteridge, *CRYSTALS User Guide*, Chemical Crystallography Laboratory, University of Oxford, 1985.
21 *International Tables for X-Ray Crystallography*, Kynoch Press, Birmingham, 1974, vol. 4.

Received 21*st November* 1990; *Paper* 0/05233G